Available online at www.sciencedirect.com
SCIENCE DIRECT®
International Journal of Heat and Mass Transfer 47 (2004) 877–886
International Journal of HEAT and MASS TRANSFER
www.elsevier.com/locate/ijhmt

Effect of pressure on the rate of evaporation from capillaries: statistical rate theory approach

P. Rahimi, C.A. Ward *

Thermodynamics and Kinetics Laboratory, Department of Mechanical and Industrial Engineering, University of Toronto, 5 King's College Road, Toronto, Canada M5S 3G8

Received 21 May 2003; received in revised form 29 August 2003

Abstract

Statistical rate theory (SRT) leads to an expression for the evaporation rate that is in terms of independently determined parameters. A series of experiments have been conducted in which water evaporated from capillaries closed at one end and partially filled to different heights. From the measured evaporation rate, the SRT prediction of the vapor-phase pressure was compared with that determined by an independent technique. When the assumptions used in this technique were valid, the value of the pressure predicted from SRT and from this technique differed by only 0.004 Pa.

Keywords: Phase change; Interfacial transport

1. Introduction

Statistical rate theory (SRT) has been proposed as a method by which the rate of molecular transport across the interface between macroscopic phases can be predicted. It has recently received significant experimental support from studies of evaporation and condensation, crystal dissolution, gas–solid surface kinetics on single crystals and on heterogeneous surfaces, and previously from gas absorption by liquids [1–23]. Evaporation is a particularly important case because the SRT expression for net evaporation flux, j_{ev} is free of any fitting-parameters [24–26]. It gives the expression for the evaporation rate in terms of the instantaneous interfacial temperature and pressure, P_I, T_I (superscripts, L or V), material properties of the substance evaporating (e.g., the saturation pressure, P_{sat}, the surface tension, γ^{SV}, and the molar specific volume, v_I) and molecular properties (internal vibration frequencies of the molecule). This relation can be inverted to obtain the expression for the interfacial vapor-phase pressure that will exist when a liquid is evaporating at a particular flux

$$P_I^V = P^V(j_{ev}, P_I^L, T_I^L, T_I^V) \tag{1}$$

In the case of water, this expression does not contain any unknown (or fitting) parameters [24,26]. Each of the parameters can be evaluated independently permitting the expression to be critically examined experimentally.

In a previous set of 15 steady state experiments with water in which P_I^V was varied from 596.0 down to 194.7 Pa giving evaporation fluxes from 0.2799 to 0.5386, g/(m^{2}s) the predictions from Eq. (1) were found to be in agreement with the measured pressure in each case to within ±13.3 Pa, the accuracy with which the vapor-phase pressure could be measured using a Hg manometer and a cathetometer [24]. When the evaporation rate of octane and methylcyclohexane were examined, the agreement between the measurements and the predictions was also good, but the test was not as rigorous, since the internal vibrational frequencies of these molecules are not known. Thus, in these cases approximations had to be made [26].

Although this seems to indicate that the SRT expression for the evaporation rate gives an accurate prediction, the expression is extraordinarily sensitive to

* Corresponding author. Tel.: +1-416-978-4807; fax: +1-416-978-7322.
E-mail address: ward@mie.utoronto.ca (C.A. Ward).

0017-9310/$ - see front matter © 2003 Elsevier Ltd. All rights reserved.
doi:10.1016/j.ijheatmasstransfer.2003.08.024

Nomenclature

J	evaporation flux, mol/(m^{2}s)
k	Boltzmann constant
m	molecular weight, molecule/(kg)
P	pressure, Pa
q_{vib}	vibrational partition function
R	radius of curvature
S	entropy
T	temperature, °C
v	specific volume, m^3/(mol)
W	molar weight, mol/kg
z	interface vertical position, mm

Greek symbols

γ^{LV}	liquid–vapor surface tension
Θ_l	characteristic temperature

Superscripts

L	liquid
V	vapor

Subscripts

B	bulk liquid–vapor interface
c	capillary interface
e	equilibrium conditions
ev	evaporation
I	interface
m	measured
sat	saturation

the vapor-phase pressure. For example, if the SRT expression for j_{ev} is written in the form

$$j_{\text{ev}} = j_{\text{ev}}(T^{\text{L}}, T^{\text{V}}, P^{\text{L}}, P^{\text{V}})$$

and the experiments described in Ref. [24] are examined, it is found when P^{V} is varied from its nominal value but within ±13.3 Pa errorbars, in some cases condensation is predicted when evaporation was measured.

To examine the SRT expression for the evaporation rate more carefully, an apparatus has been built in which the evaporation rate is measured and the pressure can be determined more accurately than ±13.3 Pa. As seen in Fig. 1, four capillaries, each closed at its lower end and each partially filled with water but to different heights, were enclosed inside a container. At the bottom of the cylindrical container, a bulk water phase was present in a concentric ring. A fifth capillary with both ends open was also present. Its lower end was immersed in the bulk water phase. To determine if equilibrium existed within the vapor phase, the height of the liquid–vapor interface in the open capillary above the liquid–vapor interface in the concentric ring could be compared with that predicted from thermodynamics. Once this equilibrium was established, there was none the less a difference in vapor-phase pressure at the liquid–vapor interfaces inside the capillaries because of the difference in height of these interfaces.

The decrease in pressure with height within the vapor phase is normally neglected, since it is only ~0.2 mPa/mm near room-temperature. However, the prediction from SRT is that there will be a measurable difference in the evaporation rate at liquid–vapor interfaces that are separated in height by only a few millimetres. Our objective in these experiments was to examine the SRT prediction of the evaporation rate for the small difference in pressure between the different half-closed capillaries.

2. Experimental apparatus, methods and procedures

The apparatus used in the experiment is shown schematically in Fig. 1. It consists of a glass container, a glass lid, an inner glass cylinder which is closed at one end and is attached to the container, and five quartz capillary tubes attached to the inner glass cylinder. One of the capillaries is open at both ends and the remaining four are closed at the lower end and open at the top. The capillaries have been attached to the inner glass cylinder in an upright position. The glass lid has fittings for attaching a pressure transducer, thermocouples, vacuum pump and a filling tube. All glass parts are made from standard weight Pyrex tubing. The dimensions of the container, inner glass cylinder and the capillaries are listed in Table 1.

All the parts were cleaned in a three stage process as described in Ref. [27]. The parts were first cleaned with acetone (Aldrich HPLC Grade), then with detergent (Alconox biodegradable) and finally with a mixture of sulfuric and chromic acid (Fisher Chromerge). A separate glass container was used to prepare the filling water. The container was cleaned following the same procedure as the apparatus. After the container was vacuumed in the last stage of cleaning, it was filled with prepared water. Then it was connected to a vacuum pump and it was vacuumed till 2/3 of the liquid water was evaporated. Experience has shown that this procedure thoroughly degasses the water.

A syringe cleaned using the same procedure as the apparatus was used to fill up the half closed capillaries to different heights without any gas being trapped inside

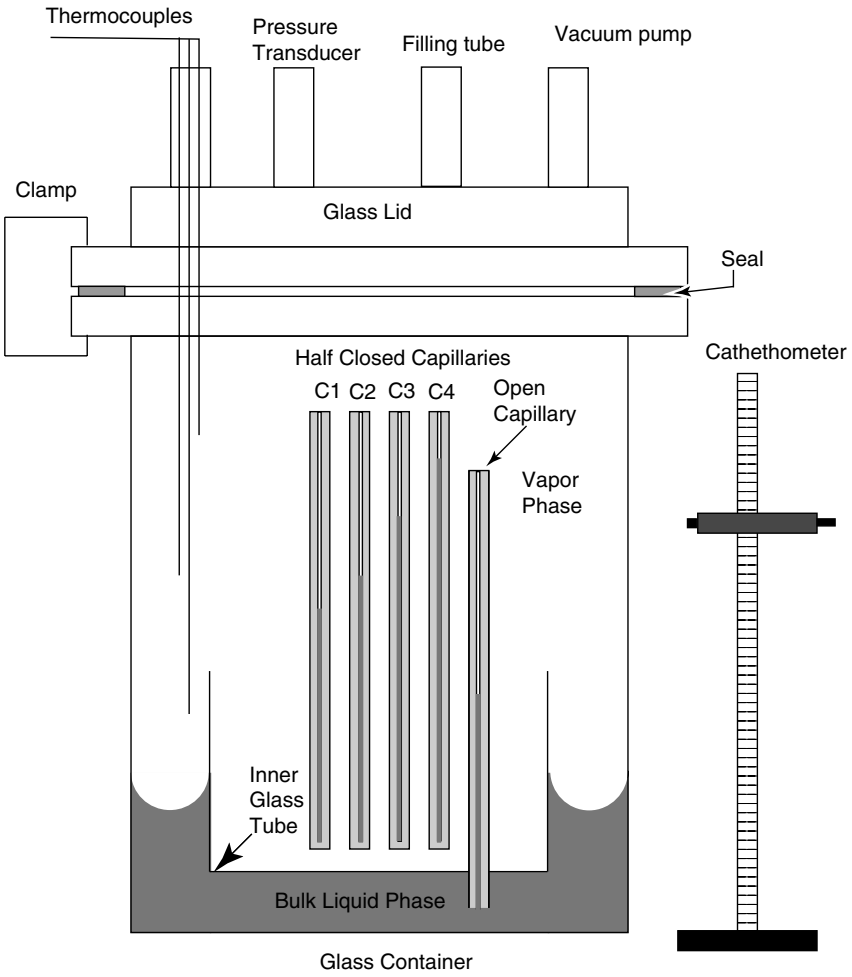

Fig. 1. Schematic of the experimental apparatus.

Table 1
Experimental apparatus dimensions

Part	Inside diameter (mm)	Outside diameter (mm)	Length (mm)
Glass container	105.94 ± 0.114	111.00 ± 0.114	200.35 ± 0.02
Inner cylinder	79.86 ± 0.057	84.94 ± 0.283	48.26 ± 0.02
Capillary tubes	1.11 ± 0.03	6.47 ± 0.02	149.31 ± 0.02

the capillaries. Then the lid was attached to the apparatus and the apparatus was sealed by means of an O-ring seal and a clamp. The apparatus was then connected to a vacuum pump and after it was vacuumed but before the liquid levels in the capillaries started to drop, the apparatus was connected to the filling container and the space between the outer and the inner glass cylinder was filled with prepared and degassed water under vacuum to a specific level (see Fig. 1). The filling container and the vacuum pump was then detached from the apparatus. The apparatus was then placed in a temperature chamber that was maintained at 5.5 ± 0.03 °C.

During the experiment, the pressure inside the apparatus was measured by a pressure transducer (OMEGA High Accuracy Absolute Pressure Transducer, PX811-005AV, with a performance accuracy of ±0.1% BFSL). Three thermocouples were used to measure the temperature at three different levels inside the apparatus (as shown in Fig. 1). The pressure transducer and the thermocouples were connected to the apparatus lid through glass openings made in the lid and were sealed

using a vacuum epoxy. The pressure transducer was calibrated against a mercury manometer and the thermocouples were calibrated with a thermometer with an accuracy of ±0.05 °C. The signals from the pressure transducer and the thermocouples were recorded every 10 s using Labview software.

Once the apparatus was inside the temperature chamber for 24 h, the position of the liquid–vapor interface inside each of the capillaries and also the bulk liquid–vapor interface were measured twice a day using a cathethometer. The accuracy with which an interface height could be measured with the cathethometer was ±10 μm. All the measurements were with respect to the bottom of the glass container.

The evaporation rates were calculated numerically from the measured height as a function of time. In doing so, a fit was made to each three consecutive measurements. The rate of the evaporation for the middle point is the slope of the fitted curve. For the last 15 measurements, a moving average method was used to calculated the evaporation rates [28].

3. Experimental results

After the system had reached thermal equilibrium with the chamber, the temperature was recorded at three different levels inside the apparatus. Each gave the same value of 5.5 ± 0.03 °C during the 35 days of the experiment. The corresponding saturation vapor pressure was 907.65 ± 1.89. The measured pressure inside the container as recorded by the pressure transducer remained constant at 914.751 ± 2.53 Pa. The interface positions as a function of time for each of the capillaries are shown in Fig. 2. As may be seen in Fig. 2, at the beginning of the experiment, the liquid inside each of the four half-closed capillaries was evaporating with different rates. The instantaneous evaporation rate in each capillary decreased with a decrease in interface position.

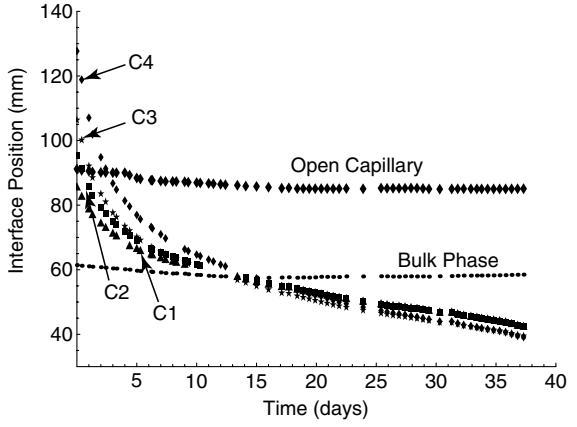

Fig. 2. Liquid–vapor interface positions within capillaries and the bulk phase that were measured during the experiment.

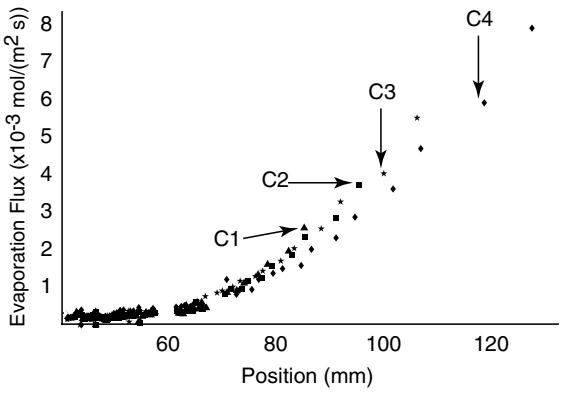

Fig. 3. Measured evaporation rate vs. measured interface position.

After several days, the interfaces in each half-closed capillary was at the same height and the rate at which each liquid phase was evaporating was the same (Fig. 2). This rate did not change further with a change in interface position. The measured evaporation rates for all the capillaries with respect to interface position are shown in Fig. 3 and are listed in Tables 2–5.

At the beginning of the experiment, there was no visible condensation inside the apparatus. But after several days, droplets had formed on the inner walls of the glass container and the inner cylinder. Also a liquid film had developed at the bottom of the inner cylinder and the film thickness grew with time.

4. Examination of the SRT expression for the evaporation flux

The SRT expression for the net evaporation flux is given in Eq. (1) or in more detailed form may be written [25]

$$j = \frac{2\eta P_{\mathrm{sat}}(T^{\mathrm{L}})}{\sqrt{2\pi m k T^{\mathrm{L}}}}\left(\sinh\left(\frac{\Delta s_{\mathrm{LV}}}{k}\right)\right) \tag{2}$$

where

$$\Delta s_{\mathrm{LV}} = k\left(4\left(1-\frac{T^{\mathrm{V}}}{T^{\mathrm{L}}}\right)+\left(\frac{1}{T^{\mathrm{V}}}-\frac{1}{T^{\mathrm{L}}}\right)\times\sum_{l=1}^{3}\left(\frac{\Theta_l}{2}+\frac{\Theta_l}{\exp(\Theta_l/T^{\mathrm{V}})-1}\right)+\frac{v_{\mathrm{sat}}^{\mathrm{L}}}{T^{\mathrm{L}}}(P^{\mathrm{L}}-P_{\mathrm{sat}}(T^{\mathrm{L}}))+\ln\left(\left(\frac{T^{\mathrm{V}}}{T^{\mathrm{L}}}\right)^4\left(\frac{P_{\mathrm{sat}}(T^{\mathrm{L}})}{P^{\mathrm{V}}}\right)\right)+\ln\left(\frac{q_{\mathrm{vib}}(T^{\mathrm{V}})}{q_{\mathrm{vib}}(T^{\mathrm{L}})}\right)\right) \tag{3}$$

and

Table 2
Experimental results for capillary C4

Day	Interface position (mm)	Measured evaporation rate $\times 10^{-3}$ (mol/(m^2 s))	Predicted vapor pressure from SRT ±0.0001 (Pa)	Calculated vapor pressure from equilibrium $\pm 10^{-6}$ (Pa)
0	127.71	7.93	907.584	907.645
2	94.83	2.88	907.625	907.648
4	81.37	1.50	907.636	907.648
6	73.27	0.92	907.641	907.649
10	64.67	0.52	907.644	907.650
12	61.59	0.47	907.644	907.650
16	55.96	0.34	907.645	907.650
18	53.67	0.37	907.645	907.650
20	52.13	0.22	907.646	907.650
22	50.02	0.31	907.646	907.650
24	48.43	0.23	907.646	907.651
26	46.61	0.18	907.647	907.651
28	45.73	0.22	907.646	907.651
30	43.98	0.29	907.646	907.651
32	43.39	0.29	907.646	907.651
34	41.92	0.20	907.646	907.651
36	39.53	0.12	907.647	907.651

Table 3
Experimental results for capillary C3

Day	Interface position (mm)	Measured evaporation rate $\times 10^{-3}$ (mol/(m^2 s))	Predicted vapor pressure from SRT ±0.0001 (Pa)	Calculated vapor pressure from equilibrium $\pm 10^{-6}$ (Pa)
0	106.36	5.53	907.603	907.647
2	83.54	2.04	907.631	907.648
4	73.49	1.17	907.639	907.649
6	67.02	0.76	907.642	907.649
10	63.89	0.45	907.644	907.650
12	56.89	0.38	907.645	907.650
16	53.84	0.31	907.646	907.650
18	51.90	0.28	907.646	907.650
20	50.53	0.31	907.646	907.650
22	48.79	0.25	907.646	907.651
24	47.47	0.20	907.647	907.651
26	45.93	0.15	907.647	907.651
28	45.22	0.18	907.647	907.651
30	43.73	0.25	907.647	907.651
32	42.78	0.20	907.646	907.651
34	41.61	0.18	907.646	907.651
36	39.67	0.10	907.647	907.651

$$\eta = \exp\left[\frac{v_{\mathrm{sat}}^{\mathrm{L}}}{kT^{\mathrm{L}}}(P_{\mathrm{e}}^{\mathrm{L}} - P_{\mathrm{sat}}(T^{\mathrm{L}}))\right] \tag{4}$$

In the above relations, $v_{\mathrm{sat}}^{\mathrm{L}}$ is the specific volume of the saturated liquid phase, k is the Boltzmann constant, T^J is the temperature at the interface in the liquid or vapor phase, $P_{\mathrm{e}}^{\mathrm{L}}$ is the pressure in the liquid under equilibrium conditions, m is the molecular mass, γ^{LV} is the liquid–vapor surface tension, R_{c1}, R_{c2} are the radii of curvature at any position on the interface, P_{sat} is the saturation vapor pressure, Θ_l is a characteristic temperature for vibration, and q_{vib} is the vibrational partition function.

In the experiment, measurements were made of j, meniscus heights in each of the four different capillaries as a function of time, T (assuming isothermal interfacial conditions) and P^{V} in the container. The measured meniscus height and the method described in Ref. [29] may be used to calculate the pressure in the liquid phase along the liquid–vapor interface. Briefly, the method is based on the assumption that liquid and vapor phases are in equilibrium and uses the differential form of the

Table 4
Experimental results for capillary C2

Day	Interface position (mm)	Measured evaporation rate $\times 10^{-3}$ (mol/(m^2 s))	Predicted vapor pressure from SRT ±0.0001 (Pa)	Calculated vapor pressure from equilibrium $\pm 10^{-6}$ (Pa)
0	95.49	3.74	907.618	907.648
2	79.41	1.58	907.635	907.649
4	71.82	0.97	907.640	907.649
6	66.56	0.43	907.645	907.649
8	64.06	0.37	907.645	907.650
10	61.67	0.38	907.645	907.650
16	55.73	0.26	907.646	907.650
18	54.05	0.25	907.646	907.650
20	52.86	0.26	907.646	907.650
22	51.33	0.20	907.646	907.650
24	50.15	0.18	907.647	907.650
26	48.74	0.13	907.647	907.651
28	48.11	0.16	907.647	907.651
30	46.71	0.23	907.647	907.651
32	45.78	0.21	907.646	907.651
34	44.61	0.16	907.647	907.651
36	42.63	0.10	907.647	907.651

Table 5
Experimental results for capillary C1

Day	Interface position (mm)	Measured evaporation rate $\times 10^{-3}$ (mol/(m^2 s))	Predicted vapor pressure from SRT ±0.0001 (Pa)	Calculated vapor pressure from equilibrium $\pm 10^{-6}$ (Pa)
0	85.39	2.59	907.627	907.648
2	74.22	1.11	907.639	907.649
3	71.06	0.86	907.641	907.649
6	64.63	0.51	907.644	907.650
7	62.92	0.29	907.646	907.650
8	62.06	0.31	907.646	907.650
16	55.27	0.23	907.646	907.650
18	53.73	0.23	907.646	907.650
20	52.63	0.26	907.646	907.650
22	51.17	0.20	907.646	907.650
24	50.03	0.17	907.647	907.650
26	48.67	0.13	907.647	907.651
28	48.02	0.15	907.647	907.651
30	46.64	0.20	907.647	907.651
32	45.68	0.20	907.647	907.651
34	44.05	0.17	907.647	907.651
36	43.09	0.11	907.647	907.651

Laplace equation to predict the shape of the interface, along with the pressure in the vapor and liquid phases across the interface. Thus, the theory may be examined by taking all of the parameters appearing in the expression for j except one to be known and then using the theory to predict the value of the remaining parameter. As pointed out in Ref. [24], to select the parameter to be predicted, it is important to consider the sensitivity of the expression for the evaporation rate on the independent variables.

The expression for the net evaporation rate that may be used to determine the variation in the evaporation rate that results from a small change in the independent variables is [24]

$$\Delta j = \left(\frac{\delta j}{\partial P^{\mathrm{V}}}\right)\Delta P^{\mathrm{V}} + \left(\frac{\delta j}{\partial T^{\mathrm{L}}}\right)\Delta T^{\mathrm{L}} + \left(\frac{\delta j}{\partial T^{\mathrm{V}}}\right)\Delta T^{\mathrm{V}} + \left(\frac{\delta j}{\partial R_{\mathrm{c}}}\right)\Delta R_{\mathrm{c}} \tag{5}$$

Eq. (5) may be written in a more detailed form

$$\frac{\Delta_j}{j} = -\frac{\Delta P^{\mathrm{V}}}{P^{\mathrm{V}}}\coth\frac{\Delta s}{k} + \left(4\left(1-\frac{T^{\mathrm{V}}}{T^{\mathrm{L}}}\right) + \frac{1}{T^{\mathrm{V}}}\sum_{1}^{3}\frac{\Theta_l \exp(\Theta_l/T^{\mathrm{V}})}{(\exp(\Theta_l/T^{\mathrm{V}})-1)^2}\right)\frac{\Delta T^{\mathrm{V}}}{T^{\mathrm{V}}}\coth\frac{\Delta s}{k} + \left(\left(\frac{h_{fg}}{kT^{\mathrm{L}}}-\frac{1}{2}\right)+\left(\frac{h_{fg}}{kT^{\mathrm{L}}}-4\right)\coth\frac{\Delta S}{k}\right)\frac{\Delta T^{\mathrm{L}}}{T^{\mathrm{L}}} - 2\frac{v_{\mathrm{sat}}^{\mathrm{L}}\gamma^{\mathrm{LV}}}{kT^{\mathrm{L}}}\frac{\Delta R_{\mathrm{c}}}{R_{\mathrm{c}}^2}\coth\frac{\Delta S}{k} \quad (6)$$

where ΔS is given in Eq. (3). To estimate the sensitivity of the rate expression to the different parameters, we may consider the capillary with the highest evaporation rate. Then the quantitative change in the evaporation flux may be calculated from the values of the parameters in this experiment

$$\frac{\Delta j}{j} = \left(-\frac{15.58}{Pa}\right)\Delta P^{\mathrm{V}} + \left(\frac{77.91}{K}\right)\Delta T^{\mathrm{L}} + \left(\frac{0.11}{K}\right)\Delta T^{\mathrm{V}} + \left(\frac{54.43}{m}\right)\Delta R_{\mathrm{c}} \quad (7)$$

If the changes in the independent variables are sufficiently small, then the most accurately measured variable during the experiment was the net evaporation flux: 0.23%. The least accurately measured variable was the vapor-phase pressure at the interface. By comparing the sensitivity of the evaporation rate to P^{V} and to T^{L}, it may be concluded that the expression for the evaporation rate is one order of magnitude more sensitive to P^{V} than to T^{L} [24]. Therefore we take the values of j, T^{V}, T^{L} and P^{L} to be the experimental values measured, and then use the SRT expression for the net evaporation rate (Eq. (2)) to predict the pressure in the vapor, P^{V} that would correspond to these conditions.

4.1. The pressure in the vapor predicted by the SRT expression

We assume the evaporation rate within each capillary to be uniform, and

$$T^{\mathrm{V}} = T^{\mathrm{L}} = T \quad (8)$$

where T is the temperature as measured by the thermocouples. This latter assumption will be examined later. When the values of P^{L}, T and measured evaporation rate j_{m} are substituted into Eq. (2), the value of the vapor-phase pressure at the liquid–vapor interface of each capillary can be predicted. The results obtained for all the capillaries are listed in Tables 2–5.

To examine the validity of the SRT expression for the rate of evaporation the predicted vapor-phase pressure from the SRT using measured value of evaporation rate should be compared with the measured value of the vapor-phase pressure. However, the vapor-phase pressure was only measured at the top of the container with an accuracy of ±3 Pa which is of insufficient accuracy to examine the predictions.

A different method is proposed for predicting the vapor-phase pressure at the liquid–vapor interface inside the half closed capillaries. In this method, liquid and vapor-phase pressures at the bulk interface, $P_{\mathrm{B}}^{\mathrm{L}}$ and $P_{\mathrm{B}}^{\mathrm{V}}$ are predicted from bulk liquid meniscus height and following a procedure described in Ref. [29]. The values of the pressure in the vapor and liquid phases at the bulk interface calculated from this procedure are listed in Table 6.

Table 6
Bulk phase and open capillary interface properties

Day	Bulk interface position ±0.01 (mm)	Calculation bulk vapor-phase pressure ±0.0001 (Pa)	Open capillary interface position ±0.01 (mm)	Calculated open capillary vapor-phase pressure ±0.0001 (Pa)
0	61.43	907.650	91.17	907.648
2	60.78	907.650	90.14	907.648
4	60.15	907.650	90.04	907.648
6	59.43	907.650	87.72	907.648
10	58.41	906.650	86.97	907.648
12	57.95	907.650	86.46	907.648
16	57.51	907.650	85.55	907.648
18	57.52	907.650	85.12	907.648
20	57.64	907.650	85.10	907.648
22	57.74	907.650	85.08	907.648
24	57.93	907.650	85.05	907.648
26	57.89	907.650	85.23	907.648
28	57.96	907.650	85.30	907.648
30	57.98	907.650	84.95	907.648
32	58.17	907.650	85.03	907.648
34	58.22	907.650	85.01	907.648
36	58.37	907.650	85.02	907.648

The pressure in the vapor-phase at the capillary interface is calculated from the vapor-phase pressure at the bulk interface, P_B^V. By knowing the distance between the bulk interface position, z_B and the capillary interface position, z_{cj} and assuming equilibrium in the vapor phase inside the container, one can find the vapor-phase pressure at the capillary interface from

$$P_{cj}^V = P_B^V \exp\left[\frac{-Wg}{\overline{R}T}(z_{cj} - z_B)\right], \quad j = 1,2,3,4 \tag{9}$$

where W is the molecular weight and $\overline{R}$ is the gas constant. The values of P_{cj}^V calculated with this procedure are listed in Tables 2–5.

As may be seen in those tables, the predicted vapor-phase pressure at the half closed capillary interfaces from the SRT expression for the rate of evaporation is in good agreement with the calculated values from the bulk-phase interface shape and assuming equilibrium in the vapor phase. The disagreement is approximately 0.004 Pa at the end of the experiment and is a maximum of 0.06 Pa at the beginning of the experiment. In order to study the reason for this change of agreement, the validity of the assumptions must be examined.

4.2. Validity of the assumptions

The assumption of isothermal conditions at the interface of the evaporating liquid inside the half closed capillaries must be examined first. In recent measurements of the temperature profile near the interface of an evaporating liquid, it was found that there is a temperature discontinuity at the interface [30]. The temperature in the vapor phase was found to be greater than that in the liquid by as much as 5 °C. The experimental data of Ref. [30] was used to predict the temperature discontinuity at the interface of the capillary with the highest evaporation rate. A temperature discontinuity of 0.5 °C was predicted to exist at the interface for the highest evaporation rate. For other evaporation rates the predicted temperature discontinuity is smaller than 0.5 °C. When this maximum temperature discontinuity was applied to Eq. (2) to predict the vapor-phase pressure, it was found that the effect of this temperature discontinuity is less than 6×10^{-4} Pa and as a result, it would not have a significant effect on the accuracy of the predicted vapor-phase pressure reported here.

The first assumption in calculating the vapor-phase pressure inside the half closed capillaries from the procedure explained in Ref. [29] is equilibrium between the liquid and vapor phases at the bulk interface. At the beginning of the experiment, even the bulk phase seemed to evaporate (though with a very small rate). This is shown in Fig. 4. It seems that only after day 15 did the bulk phase reach a state close to equilibrium.

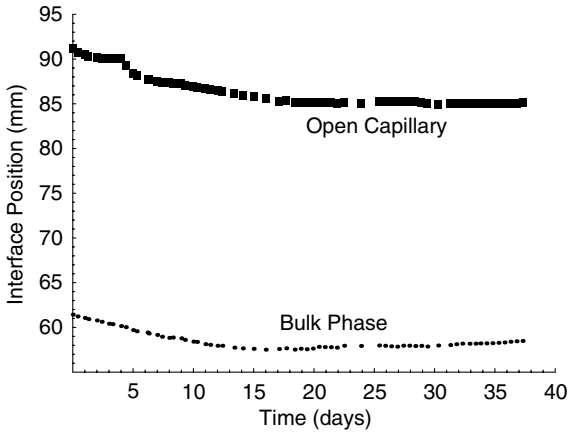

Fig. 4. Bulk liquid and open capillary liquid–vapor interface position during the experiment. Note that at the beginning of the experiment the liquid in both phases is evaporating.

The second assumption to be examined is the assumption of equilibrium in the vapor phase inside the container. This assumption can be examined by comparing the measured and predicted values of the open capillary rise ($z_B - z_{co}$) [29]. The vapor-phase pressure at the open capillary interface can be calculated by measuring the open capillary meniscus height and using the same method used in calculating the bulk phase vapor-phase pressure along the interface. A comparison between the measured capillary rise in the open capillary and that calculated from assuming equilibrium in the vapor phase inside the container is shown in Fig. 5.

As may be seen there, the vapor-phase equilibrium is not justified at the beginning of the experiment. From that plot, it seems that if the vapor-phase pressure at the

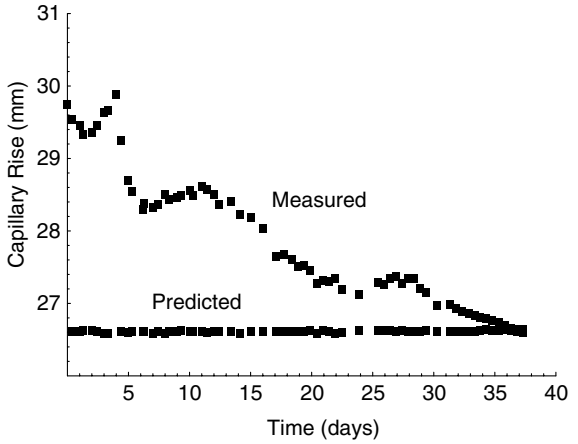

Fig. 5. Comparison between the measured capillary rise in the open capillary and that calculated from assuming equilibrium in the vapor-phase.

bulk interface is taken to be the correct value, the vapor-phase pressure at the capillary interface calculated from the assumption of equilibrium in the vapor phase is larger than the actual value. This difference is in the same direction for the half closed capillaries as may be seen in Tables 2–5. The agreement between the vapor-phase pressure at the half closed capillary interfaces predicted from the SRT expression for the rate of evaporation and that calculated from assuming equilibrium in the bulk liquid phase and in the vapor phase inside the container for the period when the assumptions are valid is around 0.004 Pa. This agreement is four orders of magnitude better than what has been reported before [24].

5. Conclusion

The apparatus constructed allowed us to show that the evaporation rate from each capillary was different with the evaporation rate being highest for the capillary with the highest interface position. Although the difference in the interface position between the capillaries C4 and C1 at the beginning of the experiment was only 42 mm (corresponding to a pressure difference of approximately 0.003 Pa), the evaporation rate of the capillary C4 was found to be three times higher than that in the capillary C1. This result supports the predictions of SRT with respect to the sensitivity of the evaporation rate to the vapor-phase pressure.

In order to calculate the vapor-phase pressure at the interfaces of the half-closed capillaries, a previously proposed method [31–35] was used. In this method the measured meniscus height of an interface is used as the boundary condition for the differential form of the Laplace equation and the pressure along the interface calculated. Once this pressure is known, the pressure in the vapor phase may be calculated, assuming equilibrium exists in this phase. The method has been successfully used to calculate the vapor-phase pressure in two different experimental studies [29,31].

When vapor-phase pressure predicted from SRT was compared with that calculated from this method, they were found to disagree by a maximum of 0.06 Pa and disagreement existed only at the beginning of the experiment. At this time, the validity of the assumption of the equilibrium in the vapor phase is questionable because the measured liquid rise in the open capillary differed with the predicted value. However, during the last 8 days of the experiment, the predicted liquid rise in the open capillary was in agreement with the measured values. Thus, during this latter period, the vapor phase appeared to be in equilibrium. And in this period, the SRT prediction of the vapor phase pressure was different from that calculated using the assumption of equilibrium in the vapor phase by only 0.004 Pa. This disagreement is four orders of magnitude less than what had been reported before [24].

Acknowledgements

The authors gratefully acknowledge the support received from the Canadian Space Agency and from the Natural Science and Engineering Research Council.

References

[1] C.A. Ward, The rate of gas adsorption at a liquid interface, J. Chem. Phys. 67 (1977) 229–235.
[2] C.A. Ward, M. Rizk, A.S. Tucker, Statistical rate theory of interfacial transport II. Rate of isothermal bubble evolution in a liquid–gas solution, J. Chem. Phys. 76 (1982) 5606–5814.
[3] C.A. Ward, P. Tikuisis, A.S. Tucker, Bubble evolution in solutions with gas concentrations near the saturation value, J. Colloid Interf. Sci. 113 (1986) 388–398.
[4] P. Tikuisis, C.A. Ward, in: R. Chabra, D. DeKee (Eds.), Transport Processes in Bubbles, Drops and Particles, Hemisphere, New York, 1992, p. 114.
[5] R.D. Findlay, C.A. Ward, Statistical rate theory of interfacial transport IV. Predicted rate of dissociative adsorption, J. Chem. Phys. 76 (1982) 5624–5631.
[6] C.A. Ward, B. Farabakhsh, R.D. Venter, Adsorption rate at the hydrogen-metal interphase and its relation to the inferred value of the diffusion coefficient, Phys. Chem. 147 (1986) 89–101.
[7] C.A. Ward, Effect of concentration on the rate of chemical reactions, J. Chem. Phys. 79 (1983) 5605–5615.
[8] C.A. Ward, R.D. Findlay, M. Rizk, Statistical rate theory of interfacial transport I. Theoretical development, J. Chem. Phys. 76 (1982) 5599–5605.
[9] C.A. Ward, R.D. Findlay, Statistical rate theory of interfacial transport III. Predicted rate of non-dissociative adsorption, J. Chem. Phys. 76 (1982) 5615–5623.
[10] C.A. Ward, M.B. Elmoselhi, Molecular adsorption at a well defined gas-solid interphase: statistical rate theory approach, Surf. Sci. 176 (1986) 457–475.
[11] J.A.W. Elliott, C.A. Ward, Chemical potential of adsorption molecules from a quantum statistical formulation, Langmuir 13 (1997) 951–960.
[12] J.A.W. Elliott, C.A. Ward, in: W. Rudzinski, W.A. Steele, G. Zgrablich (Eds.), Equilibrium and Dynamics of Gas Adsorption on Heterogeneous Solid Surfaces, Elsevier, New York, 1997, pp. 1–23.
[13] J.A.W. Elliott, C.A. Ward, Temperature programmed desorption: a statistical rate theory approach, J. Chem. Phys. 106 (1997) 5677–5684.
[14] J.A.W. Elliott, C.A. Ward, Statistical rate theory description of beam-dosing adsorption kinetics, J. Chem. Phys. 106 (1997) 5667–5676.
[15] M. Dejmek, C.A. Ward, Study of interface concentration during crystal growth of dissolution, J. Chem. Phys. 108 (1998) 8698.

[16] T. Panczyk, W. Rudzinski, A simultaneous description of kinetics and equilibria of adsorption on heterogeneous solid surfaces based on the statistical rate theory of interfacial transport, Langmuir 4 (2003) 1173–1181.
[17] T. Panczyk, W. Rudzinski, Kinetics of multi-site-occupancy adsorption on heterogeneous solid surfaces: a statistical rate theory approach, J. Phys. Chem. B 32 (2002) 7846–7851.
[18] W. Rudzinski, T. Borowiecki, T. Panczyk, Thermodesorption studies of energetic properties of nickel and nickel–molybdenum catalysts based on the statistical rate theory of interfacial transport, Appl. Catal. A 1–2 (2002) 299–310.
[19] W. Rudzinski, T. Panczyk, Remarks on the current state of adsorption kinetic theories for heterogeneous solid surfaces: a comparison of the ART and the SRT approaches, Langmuir 2 (2002) 439–449.
[20] W. Rudzinski, T. Panczyk, Kinetics of gas adsorption in activated carbons, studied by applying the statistical rate theory of interfacial transport, J. Phys. Chem. B 29 (2001) 6858–6866.
[21] W. Rudzinski, T. Panczyk, Kinetics of isothermal adsorption on energetically heterogeneous solid surfaces: a new theoretical description based on the statistical rate theory on interface transport, J. Phys. Chem. B 39 (2000) 9141–9162.
[22] W. Rudzinski, T. Borowiecki, T. Panczyk, A quantitative approach to calculating the energetic heterogeneity of solid surfaces from an analysis of TPD peaks: comparison of the results obtained using the absolute rate theory and the statistical rate theory of interfacial transport, J. Phys. Chem. B 9 (2000) 1984–1997.
[23] W. Rudzinski, T. Borowiecki, A. Dominko, A new quantitative interpretation of temperature-programmed desorption spectra from heterogeneous solid surfaces, based on statistical rate theory of interfacial transport: the effects of simultaneous readsorption, Langmuir 19 (1999) 6386–6394.
[24] C.A. Ward, G. Fang, Expression for predicting liquid evaporation flux: statistical rate theory approach, Phys. Rev. E 59 (1999) 429–440.
[25] G. Fang, C.A. Ward, Temperature measured close to the interface of an evaporating liquid, Phys. Rev. E 59 (1999) 417–428.
[26] G. Fang, C.A. Ward, Examination of the statistical rate theory expression for liquid evaporation rates, Phys. Rev. E 59 (1999) 441–453.
[27] G.B. Jackson, Applied Water and Spentwater Chemistry: Laboratory Manual, Van Nostrand Reinhold, New York, 1993, p. 65.
[28] K. Brannas, A. Hall, Estimation in integer-valued moving average models, Appl. Stochast. Models Bus. Ind. 17 (2001) 277–291.
[29] P. Rahimi, C.A. Ward, Contact angle hysteresis on smooth, homogeneous surfaces, IV, submitted for publication.
[30] C.A. Ward, F. Duan, Turbulent transition of thermocapillary flow induced by water evaporation, submitted for publication.
[31] M.R. Sasges, C.A. Ward, Effect of gravity on contact angle: an experimental investigation, J. Chem. Phys. 109 (1998) 3661–3670.
[32] C.A. Ward, D. Yee, M.R. Sasges, L. Pataki, D. Stanga, Configurational stability of fluid systems in near-weightlessness, fluid mechanics phenomena in microgravity, ASME AMD 142 (1992) 111–123.
[33] M.R. Sasges, C.A. Ward, H. Azuma, S. Yoshihara, Equilibrium fluid configuration in low gravity, J. Appl. Phys. 79 (1996) 8770–8782.
[34] C.A. Ward, M.R. Sasges, Effect of gravity on contact angle: a theoretical investigation, J. Chem. Phys. 109 (1998) 3651–3660.
[35] C.A. Ward, P. Rahimi, M.R. Sasges, D. Stanga, Contact angle hysteresis generated by the residual gravitational field of the space shuttle, J. Chem. Phys. 112 (2000) 7195–7202.